PCCP

PAPER

View Article Online
View Journal | View Issue

Cite this: *Phys. Chem. Chem. Phys.*, 2022, **24**, 8245

Accommodation of helium in $PuO_{2\pm x}$ and the role of americium

William D. Neilson,[a] Helen Steele,[b] Nikolas Kaltsoyannis[c] and Samuel T. Murphy *[a]

Received 6th December 2021,
Accepted 18th March 2022

DOI: 10.1039/d1cp05570d

rsc.li/pccp

The high alpha-activity of plutonium dioxide (PuO_2) results in significant ingrowth of radiogenic helium (He) in the aged material. To safely store/dispose PuO_2 or use in applications such as space exploration, the impact of He accumulation needs to be understood. In this work, defect energies obtained using a density functional theory (DFT) + U + D3 scheme are used in a point defect model constructed for PuO_2 to predict the method of He incorporation within the PuO_2 lattice. The simulations predict that the preferred incorporation site for He in PuO_2 is a plutonium vacancy, however, the point defect model indicates that helium will be accommodated as an interstitial irrespective of He concentration and across a wide stoichiometric range. By considering the charge imbalance that arises due to incorporation of Am^{3+} ions it is shown that He accommodation in oxygen vacancy sites will dominate in PuO_{2-x} as the material ages.

1 Introduction

The long-term management of PuO_2 stockpiles necessitates an understanding of the ageing process, particularly the impact of incorporation of decay products on the material properties. Such knowledge is also pertinent for proposed applications of PuO_2; for example, use as a component of mixed oxide fuel (MOX) or as a heat source in radioisotope thermoelectric generators. He is produced in significant quantities over storage time periods due to α-decay of Pu and a portion accumulates over time in the head space of sealed PuO_2 storage canisters.[1] The release of He from the oxide lattice has been shown to be affected by the microstructure and the presence of defects.[2] Studies have demonstrated that at temperatures typical of storage, PuO_2 pellets are able to accommodate significant amounts of radiogenic He with only small fractions released from the lattice.[2–4] Mulford *et al.*[5] studied an inventory of PuO_2 storage containers aged between 23 and 34 years, finding approximately 75% of the He produced had been retained in the oxide lattice. Similarly, Ronchi *et al.*[4] found that a 25 year old $^{239}PuO_2$ sample trapped 80–90% of its generated helium inventory. In contrast, powders in storage have exhibited much weaker retention of He, showing up to 80% of the He generated is released to the head space.

Previous theoretical investigations have employed density functional theory (DFT) to study He incorporation in $PuO_{2\pm x}$. Freyss *et al.*[6,7] report that He is accommodated on oxygen vacancies under conditions of hypo-stoichiometry, with the interstitial site favoured for PuO_2 and PuO_{2+x}. It should be noted that this study used very small (12 atom) PuO_2 simulation supercells, which typically results in poor convergence of defect formation energies. Tian *et al.*[8] introduced He into 96 atom supercells and predict that the favourable site for He is O vacancies, interstitial sites and Pu vacancies for hypo-, perfect and hyper-stoichiometry, respectively. This result relied on a point defect model (PDM) constructed for UO_2. Higher oxidation states in UO_2 allow for large hyper-stoichiometry provided by clusters of oxygen interstitials;[9] a different PDM is required to correctly describe the defect chemistry of $PuO_{2\pm x}$. PuO_2 is known to be reluctant to exist as PuO_{2+x} with small values of x predicted to be accommodated by O interstitials with Pu vacancies at concentrations several magnitudes lower.[10,11] Therefore, while helium may be easily accommodated by plutonium vacancy defects, these are likely to be rare. This work will construct a PDM for PuO_2 to investigate the mode of He incorporation within PuO_2 under a range of external conditions (oxygen partial pressure and temperature) and concentrations of He.

2 Methodology

The model adopted for the underlying PuO_2 is the longitudinal 3k anti-ferromagnetic (AFM) PuO_2 phase described by Pegg *et al.*[12]

[a] *Engineering Department, Lancaster University, Bailrigg, Lancaster, LA1 4YW, UK. E-mail: samuel.murphy@lancaster.ac.uk*
[b] *Sellafield Ltd., Sellafield, Cumbria, CA20 1PG, UK*
[c] *Department of Chemistry, The University of Manchester, Oxford Road, Manchester, M13 9PL, UK*

This model employs the Perdew–Burke–Ernzerhof exchange correlation functional revised for solids with a Hubbard correction (PBEsol + U) and spin orbit interaction (SOI) in the Vienna *ab initio* Simulation Package (VASP).[13–16] The effective on-site Coulomb (U) and exchange (J) parameters[17] were set to 7.0 eV and 0.0 eV, respectively; selected to best reproduce the ground state properties predicted by the hybrid Heyd–Scuseria–Ernzerhof (HSE06) functional.[18–21] Specifically, it was chosen to reproduce the HSE06 bandgap as the experimental data shows a large variation[22–25] and this functional has been proven to replicate experimental bandgaps.[26] The model predicts a lattice parameter of 5.415 Å in excellent agreement with the experimental value of 5.399 Å.[27]

Defect simulations were performed in a simulation supercell constructed from 2 × 2 × 2 repetitions of the unit cell using projector augmented wave (PAW)[28,29] pseudopotentials with a planewave cut-off of 500 eV, and a 2 × 2 × 2 Monkhurst–Pack k-point mesh.[30] The DFT-D3 method is used to describe the van der Waals dispersion interactions.[31] Four intrinsic defects are considered: oxygen vacancies (V_O), oxygen interstitials (O_i), plutonium vacancies (V_{Pu}) and plutonium interstitials (Pu_i). Relevant charge states for each defect are studied, modelled by adding or removing electrons from the supercell. The considered sites for He incorporation are the octahedral interstitial site (He_i) or accommodation at Pu and O vacancies (He_{Pu} and He_O, respectively) of every conceivable charge state. A visual representation of the supercell with He positioned at an octahedral interstitial site is shown in Fig. 1. The energy required to incorporate He at a interstitial site or pre-existing vacancy defect is defined as the incorporation energy:

$$E_{\text{inc}}\,(\text{He}, x) = E_{\text{He},x} - E_x - E_{\text{He}} \qquad (1)$$

where, $E_{\text{He},x}$ and E_x are the DFT energies of He at site x and an empty site x, respectively. E_{He} is the energy of an isolated He atom. The incorporation energy is insufficient to discuss the actual likelihood of incorporation of He at a given site. We therefore construct a PDM, implemented in the Defect Analysis Package (DefAP),[32] which describes a defect's concentration dependence in PuO_2 on temperature, oxygen partial pressure and quantity of He. We begin by defining a defect's formation energy:

$$\Delta G_{\text{f}}^{i} = E_{\text{def}} - E_{\text{perf}} \pm \sum_{\alpha} n_\alpha \mu_\alpha + q_i \mu_e + E_{\text{corr}} \qquad (2)$$

E_{def} and E_{perf} are the DFT total energies of the defective and perfect supercells, n_α is the number of atoms of species, α, added or removed from the system to make defect i, μ_α is the chemical potential of species α and μ_e is the electron chemical potential. Chemical potentials for Pu and O are determined according to the method described in previous work where the O chemical potential dependence on temperature is found using real gas relations.[10] A different approach is used to calculate the chemical potential of He: The total He concentration is specified and DefAP calculates μ_{He} and the blend of He defects that delivers the specified concentration of He. This is a very useful method, as the concentration of He in PuO_2 can approximated from experimental findings and/or decay equations and the information coveted is how this concentration is accommodated within the host lattice. E_{corr} is an energy correction to mitigate for finite-size effects arising due to the use of relatively small simulation supercells; the correction scheme of Kumagai *et al.*[33] is applied. In previous work on the intrinsic defect chemistry of non-stoichiometric $PuO_{2\pm x}$,[10] the contribution of vibrational entropy was also included in eqn (2). However, as there is no reliable empirical potential to describe the Pu–He interaction, which is required for the calculation of vibrational entropies, this is neglected here. Fortunately, aside from increasing the temperature at which perfect stoichiometry occurs, inclusion of vibrational entropy into the defect formation energy calculation was not found to alter which defects accommodate non-stoichiometry in $PuO_{2\pm x}$, in contrast to in UO_2.[9,34] This was true even at conditions where the vibrational entropy contribution is most significant: high temperatures. The primary influence of the vibrational entropy contribution is to decrease the favourability of the cation defects. However, in PuO_2, Pu interstitials and vacancies are found to be unfavourable, even when vibrational entropy is omitted. The vibrational entropy contribution therefore acts only to further suppress formation of these defects; omitting its contribution is, therefore, deemed acceptable.

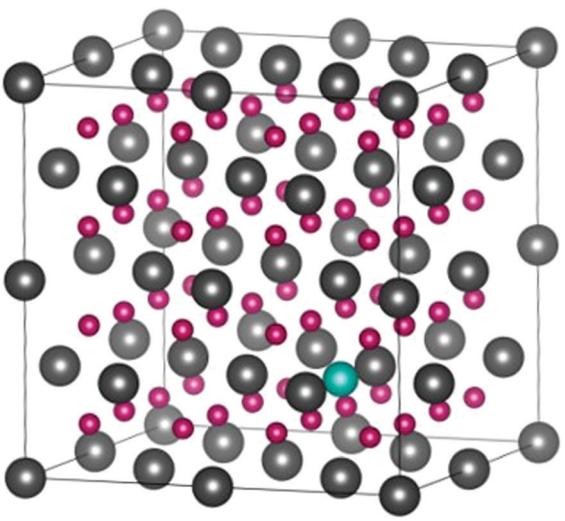

Fig. 1 The simulation supercell used for PuO_2 with a helium atom incorporated at an octahedral interstitial site. Plutonium, oxygen and helium are represented with grey, red and blue spheres, respectively.

Unlike the incorporation energy, the solution energy takes into account the population of the different accommodation sites for He and is, therefore, dependent on temperature, oxygen partial pressure and the quantity of He. The solution energy is defined as:

$$E_{\text{sol}}(\text{He}, x) = E_{\text{inc}}\,(\text{He}, x) + \Delta G_{\text{f}}^{x} \qquad (3)$$

Using Boltzmann statistics, the concentration of defect i, c_i, can be calculated using the formation energy of defect i and its multiplicity, m_i:

$$c_i = m_i \exp\left(\frac{-\Delta G_{\text{f}}^{i}}{k_{\text{B}} T}\right) \qquad (4)$$

where, k_B is the Boltzmann constant and T is the temperature. The electron chemical potential, $\mu_e = E_{\text{VBM}} + \varepsilon_F$, is expressed as

the sum of the energy of the valence band maximum (VBM), E_{VBM}, and the electron chemical potential above the VBM, ε_F (the Fermi level). DefAP employs linear bisection to find the value of ε_F that results in the system being charge neutral, thereby, satisfying eqn (5):[35]

$$\sum_i q_i c_i + \int_{-\infty}^{E_{VBM}} g_v(E) \frac{dE}{1+\exp\left(\frac{\varepsilon_F - E}{k_B T}\right)} - \int_{E_{CBM}}^{\infty} g_c(E) \frac{dE}{1+\exp\left(\frac{E - \varepsilon_F}{k_B T}\right)} = 0 \quad (5)$$

The first term in and eqn (5) is the sum of the charges of the ionic defects. The second and third terms are determined by applying Fermi–Dirac statistics to the electronic density of states (DOS) to obtain the concentrations of electrons (e^-) in the conduction band and holes (p^+) in the valence band, respectively. Eqn (5) is appropriate for a DOS that positions the VBM at 0.0 eV. Within these two integrals are g_v (E) and g_c (E), the density of electronic states in the valence band and conduction band per formula unit of PuO_2, respectively. For calculation of the electron population, E_{CBM} is the energy of the conduction band minimum. The calculated defect concentrations are used to calculate the deviation in stoichiometry. Using the concentration of a defect summed over all charge states, x in PuO_{2+x} or $-x$ in PuO_{2-x} is defined as:

$$x = \frac{2 + [O_i] - [V_O] - [He_O]}{1 + [Pu_i] - [V_{Pu}] - [He_{Pu}]} - 2$$

3 Results and discussion

In Table 1 we show the predicted incorporation and solution energies for He at different sites within PuO_2. The solution energies are dependent on environmental variables; we select a temperature of 1000 K, an oxygen partial pressure of 10^{-11} atm and a fixed He concentration of 0.001 atoms per PuO_2, conditions where PuO_2 is predicted to have perfect stoichiometry. Table 1 shows that the plutonium vacancy site is predicted to have the lowest incorporation energy for He, but the highest solution energy due to the low availability of this site at equilibrium conditions. The interstitial site has the lowest solution energy (note that the solution energy is the same as the incorporation energy as no other atoms must be displaced). In Fig. 2, the formation energies (ΔG_f^i) of the He extrinsic defects are plotted as a function of the Fermi level, at the same conditions described above for the solution energies in Table 1. The width of the x-axis corresponds the width of the band gap calculated for PuO_2 by the HSE06 and PBEsol + U (U = 7 eV) functionals, which both predict a band gap of 3.04 eV. Fig. 2 only displays the charge state of each defect that corresponds to the lowest formation energy at a given position in the bandgap. A similar plot for the intrinsic defects is given in previous work.[10] It is seen that the interstitial site is the accommodation site with the lowest formation energy across the majority of the bandgap. Only at the extremities of the bandgap, where the Fermi level is very close to the valence band or conduction band do the oxygen and plutonium vacancies have the lowest formation energy. This result suggests that it will be the interstitial site that is the preferred accommodation site for He under a wide range of conditions.

Table 1 The incorporation and solution energies for He at different sites within PuO_2. Comparison to the incorporation energy calculated in past studies is presented (Note these studies do not describe the charge state of the incorporation site). The solution energies are calculated at a temperature of 1000 K, oxygen partial pressure of 10^{-11} atm and a fixed He concentration of 0.001 atoms per PuO_2, conditions where PuO_2 is predicted to have perfect stoichiometry

		Incorporation energy (eV)		Solution energy (eV)
Site	Charge	This work	Other studies	This work
Oxygen vacancy	2+	0.38	0.34[8] −0.5[6]	3.00
	1+	0.66		3.62
	0	0.79		3.78
Plutonium vacancy	4−	0.16	0.36[8] 0.7[6]	5.05
	3−	0.16		5.78
	2−	0.16		6.80
	1−	0.16		8.01
	0	0.17		9.41
Interstitial	0	0.89	2.73[8] 0.4[6] 1.02[36]	0.89

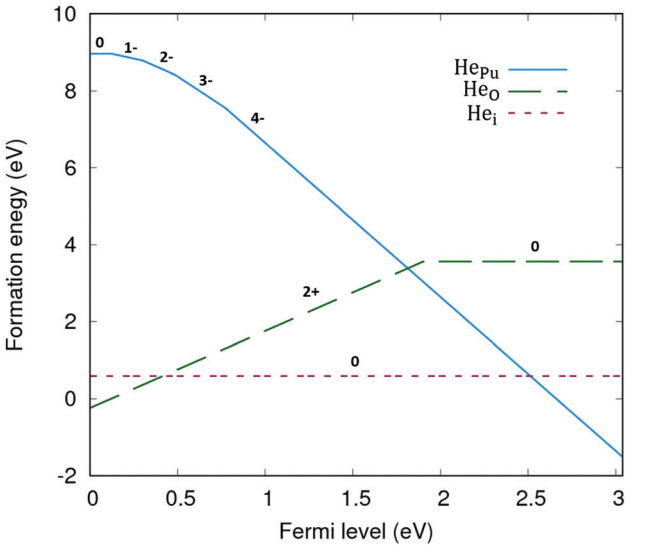

Fig. 2 Defect formation energies for He_{Pu}, He_O and He_i defects in PuO_2 as a function of the Fermi energy. Calculated at 1000 K and an oxygen partial pressure of 10^{-10} atm. Only the charge state with the lowest formation energy for a given Fermi level is shown for each defect, represented with a numeric label.

Presented in Fig. 3 is a Brouwer diagram showing the defect concentrations and value of x in PuO as a function of oxygen partial pressure at a temperature of 1000 K and fixed He concentration of 0.001 atoms per PuO_2. Multiple defects were predicted to have a concentrations of less than 10^{-15} defects per PuO_2 in the oxygen partial pressure range used, so are omitted from the plot. Fig. 3 shows that for a wide range of oxygen partial pressures encompassing both hypo- and hyper-stoichiometric conditions, the interstitial site is preferred for

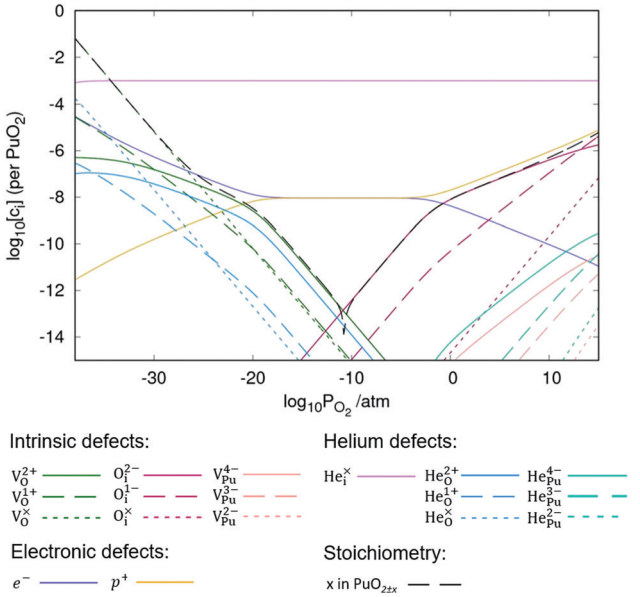

Fig. 3 Brouwer diagram showing the defect concentrations and value of x in $PuO_{2\pm x}$ as a function of oxygen partial pressure at a temperature of 1000 K and fixed He concentration of 0.001 atoms per PuO_2. To the left and right of the minima of the black line, the diagram records the calculated value of $\log_{10}[x]$ in PuO_{2-x} and PuO_{2+x}, respectively.

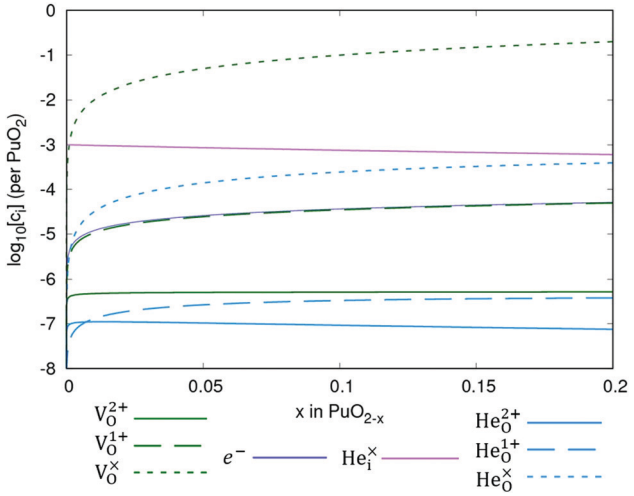

Fig. 4 The concentration of defects in PuO_{2-x} as a function of x at a temperature of 1000 K and fixed He concentration of 0.001 atoms per PuO_2.

accommodation of He. The PuO_2 PDM predicts that hyper-stoichiometry is very unfavourable; even at extremely high oxygen partial pressures, x in PuO_{2+x} never exceeds 10^{-5}. What hyper-stoichiometry there is, is accommodated by oxygen interstitials, not plutonium vacancies. Therefore, under conditions of thermal equilibrium, plutonium vacancies are an unviable accommodation site for He in PuO_2. Hypo-stoichiometry is much more favourable in PuO, and the predictions made by the PDM conform to this expectation.

Fig. 4 shows the predicted defect chemistry in PuO_{2-x} as a function of x at a temperature of 1000 K and fixed He concentration of 0.001 atoms per PuO_2. It is predicted that even at relatively large values of x in PuO_{2-x}, the interstitial site remains the preferred accommodation site for He. The amount of He accommodated on O vacancies increases with increasing hypo-stoichiometry, and the $He_O^{\times}$ defect approaches concentrations of similar magnitude to concentrations of $He_i^{\times}$, but only at significant hypo-stoichiometry.

At the VBM, of all the He extrinsic defects tested,He_O^{2+} is predicted to have the lowest formation energy at all hypo-stoichiometric conditions. The formation energy of positively charged defects increases as the Fermi level rises, whereas charge neutral defects have a formation energy that is independent of the Fermi level. In this system, the PDM predicts that the Fermi level is sufficiently high that is the He defect with the lowest formation energy for the wide range in stoichiometry tested.

The incorporation site for He is found to be independent of the total He concentration. As discussed, He is incorporated into PuO_2 as $He_i^{\times}$, or under certain conditions a proportion is $He_O^{\times}$. Both these defects are neutrally charged. Consequently, the intrinsic defect chemistry is not affected by the presence of He; the system does not need to adjust to fulfil electrical charge neutrality due to the presence of He. For the point defects investigated in this study, temperature is found not to directly affect the accommodation site for He in PuO_2, but does so indirectly by impacting the stoichiometry. Increasing temperature promotes hypo-stoichiometry, therefore the concentration of He_O defects increases with temperature, as seen in seen in Fig. 4. The heating of PuO_2 will also promote the migration and release of He from the lattice.[2]

Investigation of the ageing process of PuO_2 is incomplete without consideration of other decay products, especially americium. Aged PuO_2 contains significant ingrowth of Am produced by ^{241}Pu decaying into ^{241}Am with a half-life of 14.4 years. Am is predicted to act as a p-type dopant in PuO_2, accepting electrons and causing the Fermi level to shift towards the valence band. This could impact upon the incorporation method of He in PuO_2. In particular, a lower Fermi level could promote charged oxygen vacancies becoming the incorporation site.

To test this, we look to artificially replicate the impact Am would have in this system. We introduce a controlled concentration of charge, with a charge magnitude of -1, which replicates the accumulation of Am(III). We denote this artificial charge as λ^{1-}. In a previous study, Am(III) was found to be accommodated in PuO_2 as substitutions on Pu sites, with a net charge of -1 (Am_{Pu}^{1-}).[37] The ratio of Am(IV): Am(III) in $(Pu,Am)O_{2\pm x}$ was found to vary with external conditions and total Am concentrations. However, in conditions where Am(IV) is the dominant oxidation state, Am(III) concentrations remain high, and Am(III) is dominant in hypo-stoichiometric PuO_{2-x}, due to reduction of Am(IV).[38–40] In Fig. 5, the impact of increasing the concentration of λ^{1-} on the defect chemistry of PuO_2 is plotted, at a fixed temperature of 1000 K and oxygen partial pressure of 10^{-30} atm. We see that increasing the concentration of λ^{1-} promotes the accommodation of He on oxygen vacancies and that at a concentration of $\approx 0.01\ \lambda^{1-}$ per

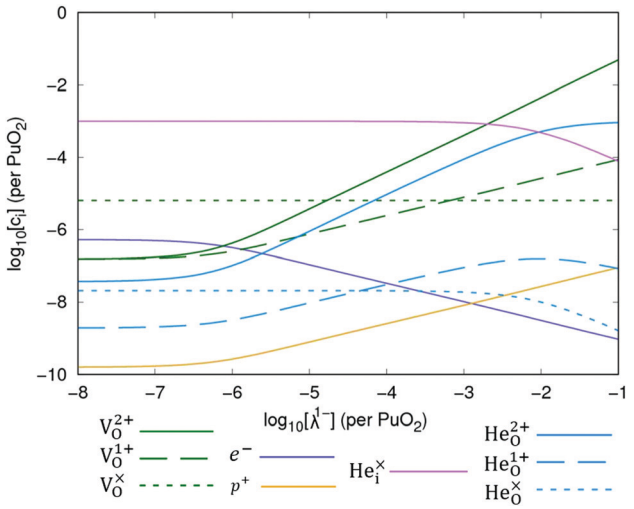

Fig. 5 The concentration of defects in PuO_2 as a function of the concentration of an artificially added charge (λ^{1-}) at a temperature of 1000 K, oxygen partial pressure of 10^{-30} atm and a fixed He concentration of 0.001 atoms per PuO_2.

PuO_2, oxygen vacancies overtake the interstitial as the site to accommodate He. Am is, therefore, likely to alter the defect chemistry of He in PuO_2 by promoting the formation of oxygen vacancies that can act as the accommodation site for He.

The final Brouwer diagram, Fig. 6, aims to predict what this all means for the interim storage of PuO_2. Fig. 6 models the defect chemistry at 500 K and a fixed concentration of 0.05 λ^{1-} per PuO_2, which simulates $\approx$5% Am(III) in PuO_2. It is now predicted that He is accommodated on oxygen vacancies under conditions of hypo-stoichiometry, with the interstitial site favoured for PuO_2 and PuO_{2+x}.

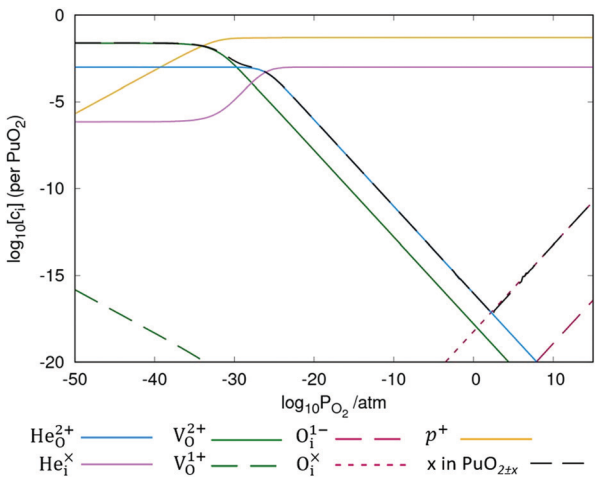

Fig. 6 Brouwer diagram showing the defect concentrations and value of x in $PuO_{2\pm x}$ as a function of oxygen partial pressure at a temperature of 500 K, and a fixed He concentration of 0.001 atoms per PuO_2. Additionally, a concentration of 5% Am(III) in PuO_2 is simulated by adding a fixed concentration of 0.05 charges (with a charge magnitude of −1) per PuO_2. To the left and right of the minima of the black line, the diagram records the calculated value of $\log_{10}[x]$ in PuO_{2-x} and PuO_{2+x}, respectively.

Our results can add to the discourse on He migration. The activation barrier for He migration *via* interstitial sites in PuO_2 will have a different activation barrier to that of migration between oxygen vacancy defect sites. Our work has predicted that the accumulation of Am promotes the formation of oxygen vacancies; we would therefore anticipate seeing a change in the barrier for He release as the material ages. We cannot quantify how it will change without calculating the barriers themselves which we leave to future work.

4 Summary

In summary, it has been shown that the preferred incorporation site for He in PuO_2 is on a plutonium vacancy. However, by considering the availability of such defects it is found using a PDM constructed for PuO_2 that accommodation of He under equilibrium conditions will be as an interstitial. This remains the preferential site regardless of the concentration of He and for values of x in PuO_{2+x} greater than −0.2. The neutrally charged $He_O^\times$ defect is the favoured oxygen vacancy for He incorporation, but its concentration in PuO_2 is found to be below that of $He_i^\times$ throughout the hypo-stoichiometric region. We consider the impact the decay product Am may have on the method of He incorporation by simulating the presence of its charge in PuO_2. We predict that increasing concentrations of Am will promote the accommodation of He on an oxygen vacancy site in hypo-stoichiometric PuO_2.

Conflicts of interest

There are no conflicts to declare.

Acknowledgements

This work was completed using the High End Computing facility at Lancaster University. The visualisation of crystal structures was performed with VESTA,[41] finite-size corrections were calculated using pymatgen.[42] This project was funded as part of EPSRCs TRANSCEND project (EP/S01019X/1).

References

1 G. Bailey, E. Bluhm, J. Lyman, R. Mason, M. Paffett, G. Polansky, G. D. Roberson, M. Sherman, K. Veirs and L. Worl, Gas Generation from Actinide Oxide Materials, LA-13781-MS, 2000.
2 T. Wiss, J.-P. Hiernaut, D. Roudil, J.-Y. Colle, E. Maugeri, Z. Talip, A. Janssen, V. Rondinella, R. J. M. Konings, H.-J. Matzke and W. J. Weber, *J. Nucl. Mater.*, 2014, **451**, 198–206.
3 M. S. El-Genk and J.-M. Tournier, *J. Nucl. Mater.*, 2000, **280**, 1–17.
4 C. Ronchi and J. P. Hiernaut, *J. Nucl. Mater.*, 2004, **325**, 1–12.
5 R. Mulford, author, Los Alamos National Laboratory, Los Alamos, NM, 2014.

6 M. Freyss, N. Vergnet and T. Petit, *J. Nucl. Mater.*, 2006, **352**, 144–150.
7 M. Freyss and T. Petit, *Ab initio modelling of the behaviour of helium in americium and plutonium oxides*, INIS-FR-3001, 2004.
8 X. Tian, T. Gao, C. Lu, J. Shang and H. Xiao, *Eur. Phys. J. B*, 2013, **86**, 179.
9 A. Soulié, F. Bruneval, M.-C. Marinica, S. Murphy and J.-P. Crocombette, *Phys. Rev. Mater.*, 2018, **2**, 083607.
10 W. D. Neilson, J. T. Pegg, H. Steele and S. T. Murphy, *Phys. Chem. Chem. Phys.*, 2021, **23**, 4544–4554.
11 Y. Lu, Y. Yang and P. Zhang, *J. Alloys Compd.*, 2015, **649**, 544–552.
12 J. T. Pegg, A. E. Shields, M. T. Storr, A. S. Wills, D. O. Scanlon and N. H. De Leeuw, *Phys. Chem. Chem. Phys.*, 2018, **492**, 269–278.
13 G. Kresse and J. Hafner, *Phys. Rev. B: Condens. Matter Mater. Phys.*, 1993, **47**, 558–561.
14 G. Kresse and J. Hafner, *Phys. Rev. B: Condens. Matter Mater. Phys.*, 1994, **49**, 14251–14269.
15 G. Kresse and J. Furthmüller, *Comput. Mater. Sci.*, 1996, **6**, 15–50.
16 G. Kresse and J. Furthmüller, *Phys. Rev. B: Condens. Matter Mater. Phys.*, 1996, **54**, 11169–11186.
17 A. I. Liechtenstein, V. I. Anisimov and J. Zaanen, *Phys. Rev. B: Condens. Matter Mater. Phys.*, 1995, **52**, R5467–R5470.
18 J. Heyd, G. E. Scuseria and M. Ernzerhof, *J. Chem. Phys.*, 2003, **118**, 8207–8215.
19 J. Heyd, G. E. Scuseria and M. Ernzerhof, *J. Chem. Phys.*, 2003, **118**, 8207–8215.
20 J. Heyd and G. E. Scuseria, *J. Chem. Phys.*, 2004, **121**, 1187–1192.
21 A. V. Krukau, O. A. Vydrov, A. F. Izmaylov and G. E. Scuseria, *J. Chem. Phys.*, 2006, **125**, 224106.
22 C. E. McNeilly, *J. Nucl. Mater.*, 1964, **11**, 53–58.
23 T. Mark McCleskey, E. Bauer, Q. Jia, A. K. Burrell, B. L. Scott, S. D. Conradson, A. Mueller, L. Roy, X. Wen, G. E. Scuseria and R. L. Martin, *J. Appl. Phys.*, 2013, **113**, 013515.
24 P. Roussel, K. S. Graham, S. C. Hernandez, J. J. Joyce, A. J. Nelson, R. Sykes, T. Venhaus and K. White, *Appl. Surf. Sci.*, 2021, **553**, 149559.
25 P. Roussel, *J. Electron Spectrosc. Relat. Phenom.*, 2021, **246**, 147030.
26 A. J. Garza and G. E. Scuseria, *J. Phys. Chem. Lett.*, 2016, **7**, 4165–4170.
27 J. M. Haschke and T. H. Allen, *J. Alloys Compd.*, 2002, **336**, 124–131.
28 P. E. Blöchl, *Phys. Rev. B: Condens. Matter Mater. Phys.*, 1994, **50**, 17953–17979.
29 G. Kresse and D. Joubert, *Phys. Rev. B: Condens. Matter Mater. Phys.*, 1999, **59**, 1758–1775.
30 H. J. Monkhorst and J. D. Pack, *Phys. Rev. B: Condens. Matter Mater. Phys.*, 1976, **13**, 5188–5192.
31 S. Grimme, J. Antony, S. Ehrlich and H. Krieg, *J. Chem. Phys.*, 2010, **132**, 154104.
32 S. T. Murphy and N. D. M. Hine, *Chem. Mater.*, 2014, **26**, 1629–1638.
33 Y. Kumagai and F. Oba, *Phys. Rev. B: Condens. Matter Mater. Phys.*, 2014, **89**, 195205.
34 M. W. Cooper, S. T. Murphy and D. A. Andersson, *J. Nucl. Mater.*, 2018, **504**, 251–260.
35 M. Youssef and B. Yildiz, *Phys. Rev. B: Condens. Matter Mater. Phys.*, 2012, **86**, 144109.
36 D. Gryaznov, S. Rashkeev, E. A. Kotomin, E. Heifets and Y. Zhukovskii, *Nucl. Instrum. Methods Phys. Res., Sect. B*, 2010, **268**, 3090–3094.
37 W. D. Neilson, H. Steele and S. T. Murphy, *J. Phys. Chem. C*, 2021, **125**, 15560–15568.
38 M. Osaka, K. Kurosaki and S. Yamanaka, *J. Nucl. Mater.*, 2006, **357**, 69–76.
39 R. C. Belin, P. M. Martin, J. Lechelle, M. Reynaud and A. C. Scheinost, *Inorg. Chem.*, 2013, **52**, 2966–2972.
40 T. Matsumoto, T. Arima, Y. Inagaki, K. Idemitsu, M. Kato, K. Morimoto and T. Sunaoshi, *J. Nucl. Sci. Technol.*, 2015, **52**, 1296–1302.
41 K. Momma and F. Izumi, *J. Appl. Crystallogr.*, 2011, **44**, 1272–1276.
42 S. P. Ong, W. D. Richards, A. Jain, G. Hautier, M. Kocher, S. Cholia, D. Gunter, V. L. Chevrier, K. A. Persson and G. Ceder, *Comput. Mater. Sci.*, 2013, **68**, 314–319.

